Proceedings of the IASS 2024 Symposium
Redefining the Art of Structural Design
August 26-30, 2024, Zurich Switzerland
Philippe Block, Giulia Boller, Catherine DeWolf,
Jacqueline Pauli, Walter Kaufmann (eds.)

Reliable experimental testing methodology for reciprocal structures

Martin STEINMETZ*, Luca SGAMBI[a], Pierre LATTEUR[b]

* UCLouvain, Louvain Research Institute LAB
1340 Louvain-la-Neuve, Belgium
martin.steinmetz@uclouvain.be

[a] UCLouvain, Louvain Research Institute LAB
1340 Louvain-la-Neuve, Belgium

[b] UCLouvain, iMMC
1340 Louvain-la-Neuve, Belgium

Abstract

Reciprocal structures are known to resemble "pick-up sticks" due to their architectural appearance devoid of apparent hierarchy. They consist of elements that are both supporting and supported, thereby complicating both their design and construction, as well as their structural analysis. Paradoxically, they are infrequently constructed despite the abundant scientific literature. This imbalance is partly explained by the fact that this literature mainly addresses geometric aspects without delving into the stability rules and modelling of connections and supports. Only a few researchers have undertaken experimental tests to validate their numerical models, yielding inconclusive results. They have notably highlighted the difficulty of measuring and modelling the behaviour of connections between beams. This article is part of a comprehensive effort to define and experimentally validate complex reciprocal structure stability, design, and calculation rules. Specifically, it outlines a reliable experimental methodology, including the testing protocol and setup, as well as data collection and post-processing. It is applied to an elementary planar reciprocal structure composed of three circular steel tubes, whose simplicity facilitates modelling, measurement and conclusions. The objective is to validate this methodology before applying it to more complex reciprocal structures.

Keywords: Reciprocal structure, Laboratory tests, Testing guidelines.

1. Introduction

According to Geno et al. [1] and Parigi and Kirkegaard [2], a reciprocal structure (RS) is a 2D or 3D structure formed by the repetition of one or more basic modules, following these fundamental rules (Figure 1) :

- A basic module consists of at least three beams.
- Each beam is supported at its ends, either by two other beams or by another beam and one support.
- Each beam supports at least one other beam.

Among the advantages of reciprocal structures, the following should be mentioned:

- Architectural aesthetics associated with an unusual aspect without a clear hierarchy [3].
- Spanning large distances using elements of short lengths, which is beneficial, for example, for wooden log elements [4].
- Assemblies connect only two elements simultaneously [5].

However, reciprocal structures can also present significant challenges:

- Geometric design is iterative: the movement of a single node or beam influences the position of all others and disrupts overall geometric compatibility. Nonetheless, geometric design has been extensively documented, and several design methods have been proposed [6–8], some of which are integrated into parametric drawing software [2].
- Confidence in numerical models' results, as they are strongly influenced by the behaviour of assemblies, of which the design and modelling are complex [9-10].
- Construction and assembly phases are complex [6].

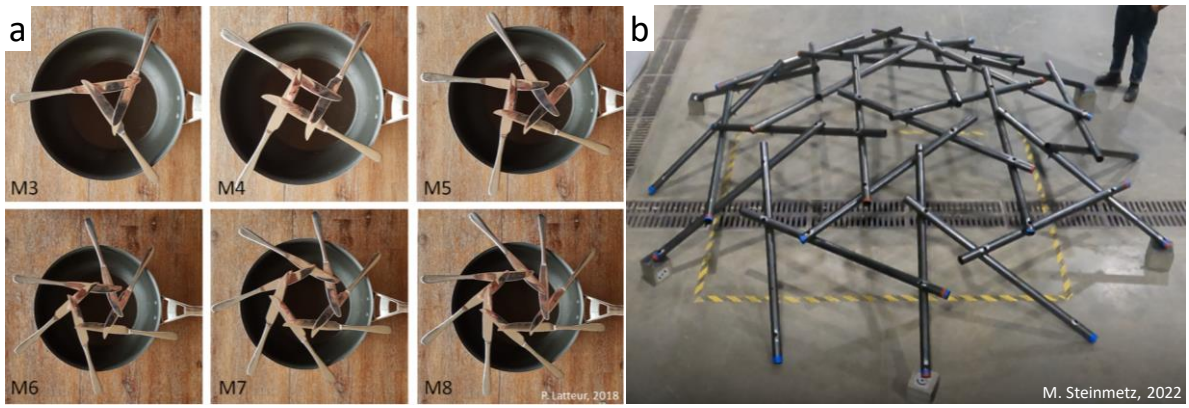

Figure 1: a) A simple reciprocal module comprising 3 to 8 elements. b) A complex reciprocal structure constructed by the authors.

These drawbacks explain why a low number of RSs have been constructed to date, especially 3D structures composed of more than one module [3]. The main challenge concerns the reliability of numerical modelling, mainly that of assemblies, as presented in [10–13]. These authors conducted experimental studies on RSs, summarised below, to validate their models using measurements of displacements and strain deformations.

The RS from the first study presented in Rizzuto and Hulse [11] and Rizzuto [12] is depicted in Figure 2a and generated by rotating all the edges of a dodecahedron by the same angle, with the axis of rotation passing through the centre of the volume and the midpoint of each edge. The choice of the dodecahedral shape ensures a uniform geometry such that all circular steel tubes are identical in diameter and length and have identical eccentricity and position of connections. The assembly between the tubes is done through bolts passing through both sections, with intermediate saddleback washers conforming to the curvature of the two tubes to improve load transfer at the interface (Figure 2b). Cyclical loading is transmitted to the upper module through a plate on the bolt heads. The lower module is in contact with a support plate, placed similarly. Some tube end displacements are measured using LVDTs placed along the tube axis. Additionally, rosette strain gauges are placed on the tubes sufficiently far from the assemblies and the tube's longitudinal welded seam to avoid measurement disturbance. The experimental measurements concerning symmetrically placed tubes differ by up to 11.8% regarding strain deformations. Also, the numerical results overestimate the measured displacements by 9.3%.

The RS from the second study presented in Rizzuto [10, 13] is designed from a honeycomb dome, which has the advantage of having a mesh connecting only three edges at a time and whose face area is globally constant over the dome surface (Figure 2c). Each edge is rotated at the same angle around an axis passing through its centre and the dome's origin. Then, an algorithm based on dynamic relaxation is used to ensure the same eccentricity between the steel tubes while preserving radial symmetry in five sectors. The assembly between the tubes is identical to that of the previous study. The tubes' ends in contact with the steel support are horizontally cut, limiting horizontal displacement during loading only by friction. The load is transferred to the centre of the two upper tubes through a distribution beam and applied in increasing steps. LVDTs are placed at specific tube ends to measure vertical displacement, and rosette strain gauges, for computing pointwise von Mises stresses, are positioned halfway between the connection zones to avoid stress concentration zones. The experimental results were compared to

different numerical models, varying the modelling assumptions of supports and connection. None of the models could simultaneously provide a satisfactory displacement and stress distribution prediction.

For these two studies, the authors reported difficulties in capturing accurate measurements despite well-thought-out and ingenious experimental setups. These difficulties are caused by i) the movement at support points, ii) structure displacements showing components in all three directions, and iii) the presence of all internal forces in beams influencing strain measurements.

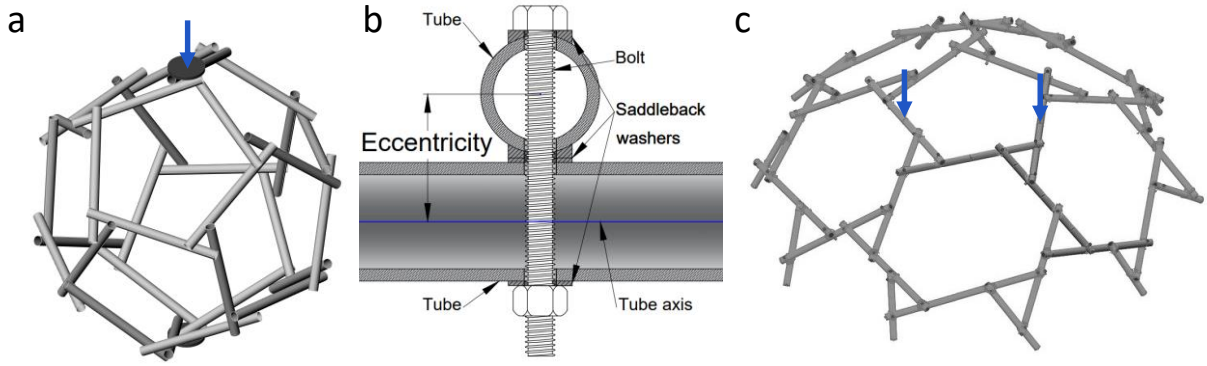

Figure 2: Reciprocal structures tested in the literature: a) generated from a dodecahedron [11, 12]; b) circular tube assembly; c) generated from a honeycomb dome [10, 13]. Figures are redrawn based on the cited studies.

This article proposes best practice guidelines for future testing campaigns on complex RSs tested in a laboratory setup. Based on the difficulties presented in the literature, solutions are proposed to facilitate comparison between measurements and numerical results. To achieve this goal, as a preliminary step, the authors numerically modelled and then laboratory-tested a RS consisting of three steel tubes located in the same plane. The chosen structure is deliberately simple, enabling reliable modelling compared to confident experimental results.

Section 2 presents the tested SR prototype, test setup, loading procedure, measurement, and associated numerical model. The post-processing of strain gauge measurements is developed in Section 3. Experimental measurements and numerical results are presented in Section 4 and discussed in Section 5. Finally, the conclusion outlines, based on this test and those in the literature, the best possible practice guidelines to obtain reliable measurements and facilitate correspondence with the numerical model for future tests on more complex structures.

2. Description of experimental design and numerical model

The tested prototype, depicted in Figure 3, ensures radial symmetry, with its centre passing through the actuator's axis. It comprises three laterally connected tubes in the horizontal plane (Figure 3a). Each tube (denoted A, B, and C) is 2000 *mm* long and has a 60.3×2.9 *mm* section.

To assemble the structure, the supporting tube is drilled at a 60° angle with a 19 *mm* diameter hole (Figure 3b) to accommodate an 18 *mm* diameter rod (steel 8.8). This rod is fixed to the end of the supported tube through a welded plate of 19 *mm* thickness (Figures 3c and 3f). At the supports, the tube is laterally welded to a support plate placed on a roller (Figure 3e). The connections and supports were chosen to be as ideal as possible while ensuring the stability of the structure.

The instrumentation is placed identically on each tube to maintain radial symmetry in measurement. The vertical component of the structure's displacement is measured at three points at the assembly location using LVDTs (Figure 3c). On each tube, six strain gauges (SGs) are glued along the perimeter of the same cross-section (Figure 3d) to determine the intensity and position of the maximum von Mises stress. This measurement section is located halfway between the connection zone and the support to limit disturbances from these singularities and ensure the Saint-Venant principle. The post-processing of strain gauge measurements into internal forces and then into von Mises stresses is explained in Section 3.

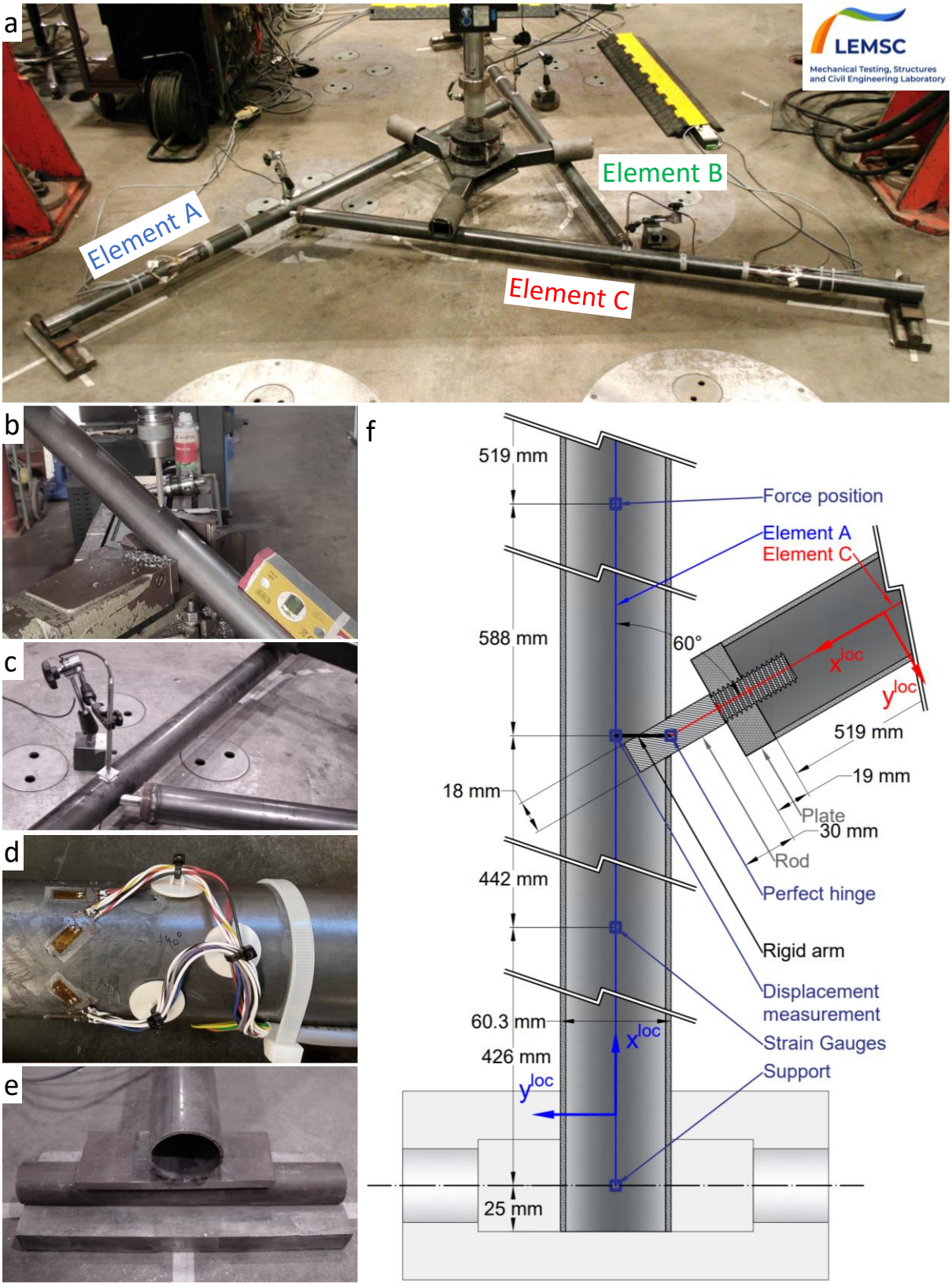

Figure 3: (a) The laboratory-tested reciprocal structure prototype. Details of the assemblies (c) and supports (e). Displacement sensors (LVDT) are visible in detail (c), and the arrangement of strain gauges is shown in detail (d). Detail (b) illustrates the assembly's drilling. Detail (f) specifies the geometrical data for the numerical modelling.

The numerical model is built using the commercial software "SCIA Engineer" following the scheme presented in Figure 3f. The tubes are modelled using "Timoshenko" beam-type elements. Each beam accounts for the diameter change at its end, at the connection zone. Its local axis x^{loc} is directed along the axis of the tube towards the center of the structure, its local axis z^{loc} is vertical, and its local axis y^{loc} is determined by the right-hand rule (Figure 4a). The node is assumed to be pinned at the contact point between the rod and the supporting tube. A fictive rigid arm, corresponding to the radius of the supporting tube, connects the pin to the axis of the supporting tube. At the support, rotation around x^{loc} and translation along z^{loc} are constrained. Due to friction and considering that the loading is purely vertical, translation along y^{loc} is also assumed constrained.

3. Post-processing of strain gauge measurements

At a particular cross-section of a steel tube, six strain gauges glued along the perimeter enable the determination of internal forces F^{loc} and M^{loc} according to the local coordinate system, as defined in Figure 4a. Based on the internal forces, the maximum von Mises stress and its position can be calculated.

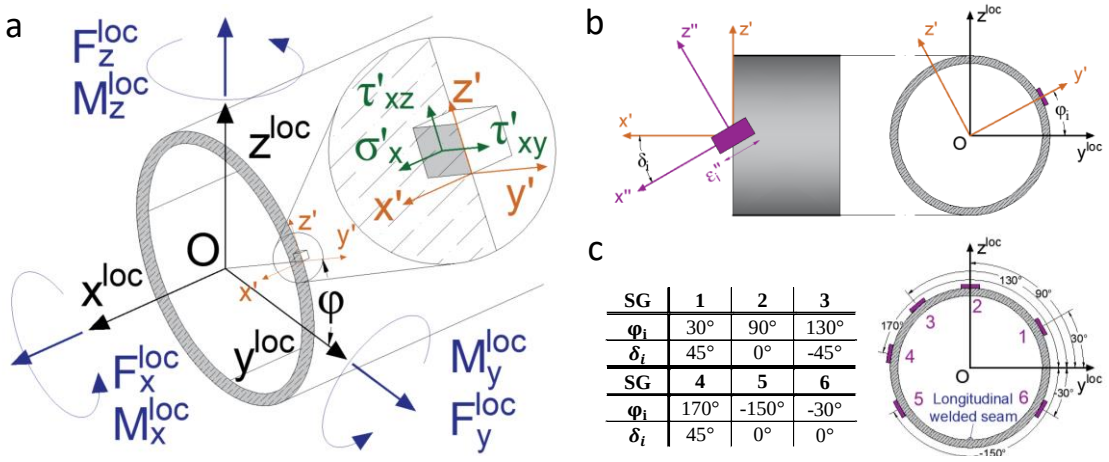

SG	1	2	3
φ_i	30°	90°	130°
δ_i	45°	0°	-45°
SG	4	5	6
φ_i	170°	-150°	-30°
δ_i	45°	0°	0°

Figure 4: (a) Internal forces in the local coordinate system, presented in their positive direction: the normal force F_X^{loc}, the shear forces F_Y^{loc} and F_Z^{loc}, the torsional moment M_X^{loc}, and the bending moments M_Y^{loc} and M_Z^{loc}. The normal stresses σ_x', and the shear stresses τ_{xz}', and τ_{xy}', in the x'y'z' coordinate system are indicated for any point along the perimeter, depending of the position angle φ. (b) Convention for the position angles φ_i and orientation angles δ_i for strain gauges. (c) Table and representation of the angles of the six strain gauges (SG from 1 to 6) along the same cross-section.

First, the strain of a single strain gauge glued to the outside of the tube is analysed. Initially, the position angle φ_i and orientation angle δ_i of the gauge, defined in Figure 4b, and the material and geometric properties of the steel tube, defined in Table 1, were determined. During the test, the strain ε_i'' measured by this gauge is theoretically a function of the six local internal forces existing in the considered cross-section. Iriarte et al. [14] give it for circular steel tubes in Equation 1.

$$\varepsilon_i''(\varphi_i, \delta_i, F^{loc}, M^{loc}) = \left(\frac{1-(1+\nu)sin^2\delta_i}{E.A}\right)F_X^{loc} + \left(\frac{(1+\nu)sin(2\delta_i).sin\varphi_i}{k.E.A}\right)F_Y^{loc}$$
$$+\left(-\frac{(1+\nu)sin(2\delta_i).cos\varphi_i}{k.E.A}\right)F_Z^{loc} + \left(-\frac{(1+\nu)sin(2\delta_i)}{E.I_p/R}\right)M_X^{loc}$$
$$+\left(\frac{(1-(1+\nu)sin^2\delta_i)sin\varphi_i}{E.I/R}\right)M_Y^{loc} + \left(-\frac{(1-(1+\nu)sin^2\delta_i)cos\varphi_i}{E.I/R}\right)M_Z^{loc} \quad (1)$$

This equation can be vectorially represented as $\varepsilon_i'' = [w_i][F]$, where the row vector $[w_i]$ regroups the terms E, A, k, I, I_p, R, ν, φ_i and δ_i, and the column vector $[F]$ contains the six internal forces. This relation can be generalized in matrix form, as presented in Equation 2, in the case where the six SGs are placed along the same perimeter.

$$\begin{bmatrix} \varepsilon''_1 \\ \varepsilon''_2 \\ \varepsilon''_3 \\ \varepsilon''_4 \\ \varepsilon''_5 \\ \varepsilon''_6 \end{bmatrix} = \begin{bmatrix} [w_1] \\ [w_2] \\ [w_3] \\ [w_4] \\ [w_5] \\ [w_6] \end{bmatrix} \begin{bmatrix} F_X^{loc} \\ F_Y^{loc} \\ F_Z^{loc} \\ M_X^{loc} \\ M_Y^{loc} \\ M_Z^{loc} \end{bmatrix} \tag{2}$$

The six internal forces can then be determined by inverting the matrix composed of the vectors $[w_i]$. To ensure that this square matrix is invertible, the position and orientation angles of the six SGs selected in this study are indicated in Figure 4c. Other combinations of angles are proposed by Iriarte et al. [14]. However, care must be taken not to position a SG on the longitudinal welded seam of the tube to avoid measurement disturbance.

Table 1: Material and geometric properties of the circular steel tubes.

	Property	Indication	Value	Unit
Material	Young's Modulus	E	210000	MPa
	Yield strength	$f_{y,k}$	235	MPa
	Poisson's Ratio	ν	0.3	-
Geometric	Outer Radius	R	30.15	mm
	Inner Radius	r	27.25	mm
	Area	$A = \pi(R^2 - r^2)$	523	mm^2
	Moment of Inertia	$I = \frac{\pi}{4}(R^4 - r^4)$	215924	mm^4
	Polar Moment of Inertia	$I_p = \frac{\pi}{2}(R^4 - r^4)$	431848	mm^4
	Radius Ratio	$m = r/R$	0.904	-
	Shear Coefficient	$k = \frac{6(1+\nu)(1+m^2)^2}{(7+6\nu)(1+m^2)^2 + (20+12\nu)m^2}$	0.533	-

Finally, the internal forces allow determining the intensity and position of von Mises stresses on the perimeter of the tube, denoted as σ_{vM}, which are expressed in (the only non-null) terms of normal stresses σ'_x (Equation 3) and shear stresses τ'_{xz} (Equation 4) defined in Figure 4a: $\sigma_{vM} = \sqrt{(\sigma'_x)^2 + 3(\tau'_{xz})^2}$. These two stresses depend on the position of the point considered along the perimeter defined by the angle φ.

$$\sigma'_x = \frac{+F_x^{loc}}{A} + \frac{-M_y^{loc}.sin\varphi + M_z^{loc}.cos\varphi}{I/R} \tag{3}$$

$$\tau'_{xz} = \frac{+M_x^{loc}}{I_p/R} + \frac{-F_y^{loc}.sin\varphi + F_z^{loc}.cos\varphi}{k.A} \tag{4}$$

The maximum intensity $\sigma_{vM,Max}$ and its position angle φ_{Max} along the perimeter can then be deduced.

4. Experimental measurements and numerical results

The cyclically vertically applied actuator force F is divided symmetrically and equally into three points through a distribution piece (Figure 3a) with an actuator load speed of 1.8 *mm/min*. The latter ensures sufficient measurement points (>~700/cycle) and is deduced based on the expected total displacement and the maximum acquisition rate given the number of instrumentations. The loading protocol is illustrated in Figure 5a:

- The pre-loading consists of the first eight cycles (cycles 1 to 8, in grey), aimed at setting up the structure and compensating for the clearance in the connections, with a maximum force $F_{Max} = 2.25\ kN$ for cycle 7 and 8. The maximum force is limited to prevent yielding by ovalisation at the lateral connection zones, occurring for $F > 3\ kN$.
- The post-processed loading corresponds to the last five cycles (cycles 9 to 13, in black) of loading and unloading with an actuator force ranging from 0.25 *kN* to 2.25 *kN*.

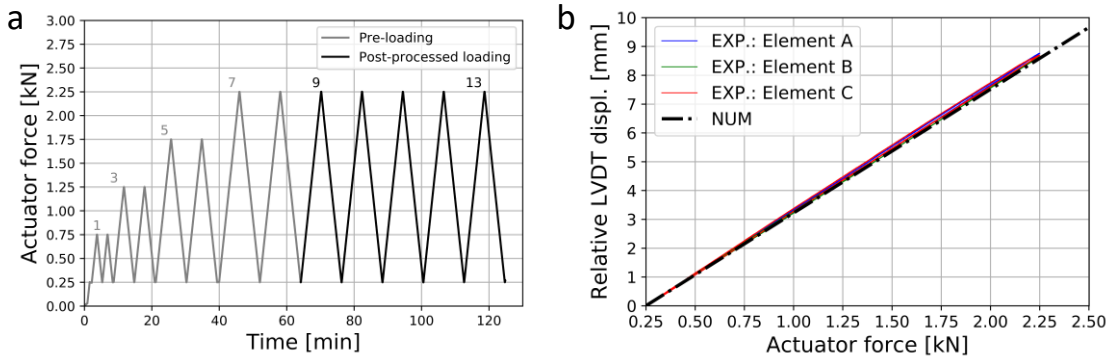

Figure 5: (a) The loading protocol comprises pre-loading cycles (in grey) and post-processed loading cycles (in black). (b) Relative vertical displacement of tubes A, B, and C at the connection zones for the post-processed loading.

The measurements from cycles 9 to 13 are superimposed on Figures 5b, 6 and 7. To remove the influence of the structure's settlement caused by the pre-loading, the measurements are indicated relative to the values at the beginning of cycle 9. The results of the numerical model are shown with a discontinuous line. The following comments can be made:

- Values of vertical displacements measured by the LVDTs are shown in Figure 5b. The maximum displacements of the three tubes are very similar, with a maximum deviation of less than 0.7% (tube A) around the average of the three peak measurements (8.7 *mm*). The observed behaviour is linear with slight hysteresis (no variation between cycles) and low residual displacement ranging from 0.03 to 0.05 mm for the tubes over all five cycles. The numerical model predicts a maximum (relative) displacement of 8.58 mm for an equivalent actuator force of 2.25 *kN*.
- Calculated from measurements at the strain gauges, Figure 6 provides the value of the three theoretically non-zero internal forces (M_y^{loc}, M_x^{loc} and F_z^{loc}). The right axis indicates the corresponding equivalent stress, σ_x or τ_{xz}. At F_{Max}, the moment M_y^{loc} contributes, as expected, significantly to the relative internal stresses (respectively 40.17 *MPa*, 40.71 *MPa*, and 40.53 *MPa* for tubes A, B, and C), compared to M_x^{loc} and F_z^{loc}. The numerical model correctly indicates the trend and magnitude of the three internal forces. For M_y^{loc}, it predicts a maximum relative internal stress of 39.69 *MPa* for an equivalent actuator force of 2.25 *kN* (corresponding to a difference of 2% with experimental measurements, on average).

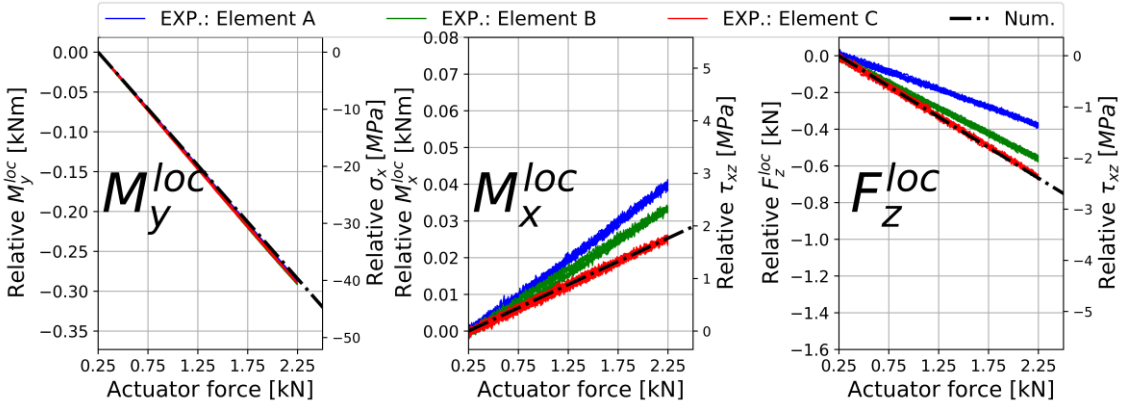

Figure 6: (from left to right) Internal forces, M_y^{loc}, M_x^{loc} and F_z^{loc} in the local coordinate system for tubes A, B, and C.

- Figure 7 provides the value and angular position of the relative maximum von Mises stress. The position is indicated based on the angle φ relative to the y^{loc} axis. The relative maximum stresses of the tubes vary with a maximum deviation of less than 0.5% around the average of the three measurements (41.09 *MPa*), slightly higher than the numerical value of 39.82 *MPa*. The positions of these maximum stresses are −89.76°, −90.25°, and −89.39° for tubes A, B, and C, respectively, and −90.46° for the numerical model at maximum force. The switch position of the maximum stress from the lower to the upper surface is linked to the sign change of the theoretically zero internal forces F_x^{loc}, F_y^{loc} and M_z^{loc} discussed in the following section.

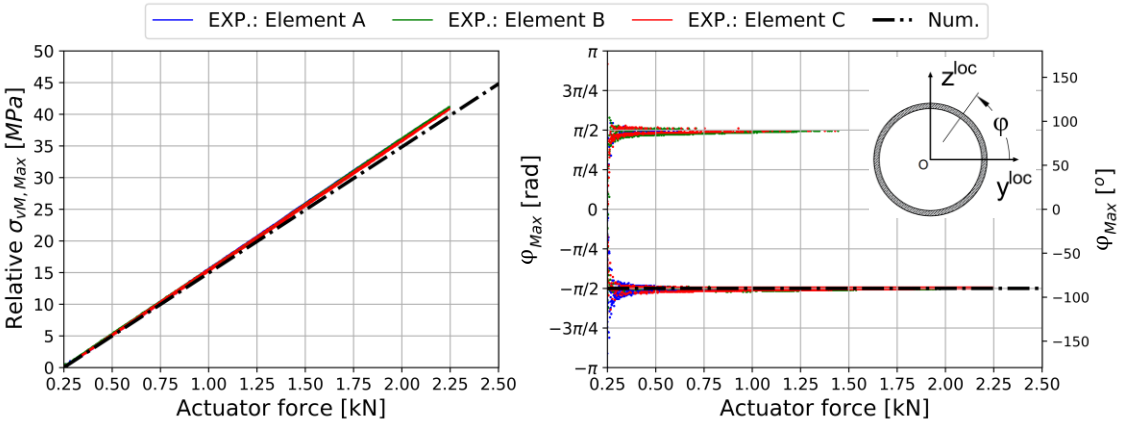

Figure 7: (left) Maximum von Mises stress on the section and (right) localisation of the maximum stress based on the angle φ, for tubes A, B, and C.

5. Discussion

The numerical model accurately predicts the tested structure's behaviour, thus confirming the proposed experimental approach and the strain gauge measurement post-processing procedure. However, some comments can be made regarding the measurements and the difference with the numerical results :

- Concerning the vertical displacements of the nodes, the numerical model results exhibit a slightly stiffer behaviour than the measurements. The maximum differences are 2.1%, 0.74%, and 1.38% for tubes A, B, and C, respectively.
- As for internal forces, M_x^{loc} and F_z^{loc} of the three tubes are noticeably different despite the radial symmetry. However, in contrast to the stresses generated by the moment M_y^{loc} of the three tubes, this difference is slight in the absolute magnitude.
- The theoretically zero internal forces F_x^{loc}, F_y^{loc} and M_z^{loc} are depicted in Figure 8. The occurrence of non-zero measurements is likely explained by the appearance of eccentricity between the tubes and the support roller's axis (Figure 3e), which causes parasitic force components in the OXY plane (second-order effect not accounted for in the numerical model). The magnitude of these internal

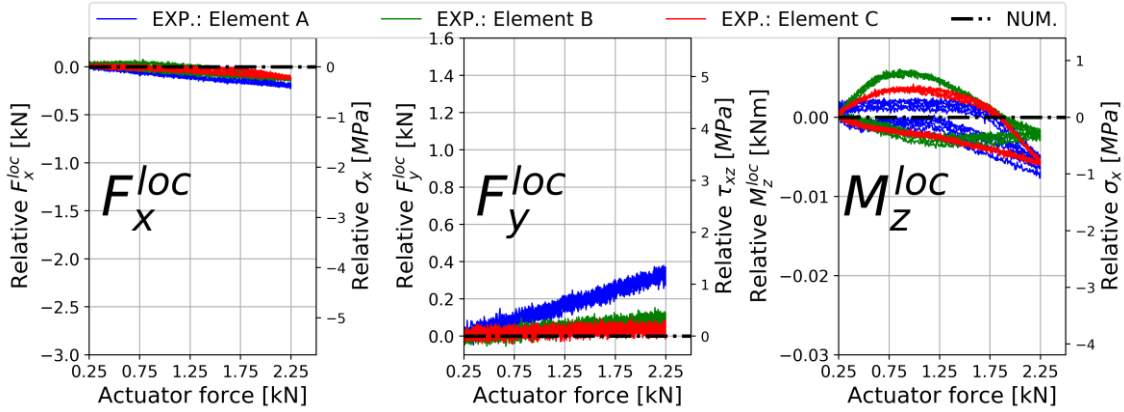

Figure 8: (from left to right) Measurement of the internal forces F_x^{loc}, F_y^{loc} and M_z^{loc}, theoretically zero, for tubes A, B, and C.

forces is low but sufficiently significant (e.g. M_z^{loc}) to influence the computation of the von Mises stress and its position.
- Concerning the intensity and position of the maximum von Mises stress, the previous observation explains that its maximum measured intensity is slightly more overestimated than considering only M_y^{loc} (3 % instead of 2%, on average), and its position is slightly shifted compared to the numerical responses. Also, the change in signs of the different internal forces influences the position of the maximum stress. However, on average, experimental measurements and numerical results differ only from a maximum of 1.1% in angle for high applied forces.

6. Conclusion and best practice guidelines for testing

Reciprocal structures (RSs) pose significant challenges in design, modelling, construction, and experimental testing. During testing, the literature highlights difficulties in measurement as reciprocity generates beam displacements with components in all three directions, and the presence of axial forces, bi-axial bending, shear, and torsion in beams influences strain gauge measurements.

This article aligns with the authors' broader aim of validating numerical models of more complex RSs by comparing numerical results to measurements on prototypes tested in the laboratory. To achieve this, as a preliminary step, the authors numerically modelled and then experimentally tested a RS consisting of three circular steel tubes. While deliberately elementary, the selected structure design demonstrated a good correspondence with experimental measurements, confirming the methodology outlined. Based on the test conducted in this article and the challenges presented in the literature, the following best practice guidelines are recommended:

Regarding the testing setup:

- Prefer symmetry in the structure, loading, and sensor positioning whenever possible, as it allows for redundant measurements. Construction and assembly of the structure will also be facilitated.
- Idealize the supports of the tested structure to facilitate their modelling. For 2D RSs, a solution is proposed in Figure 3e. For 3D RSs, a proposal is to weld a half-sphere to the tube ends at the supports and place them in a holder (Figure 9a). This way, all three translations are constrained (in compression) while allowing tube rotation. The position of the pinned support in the model is at the centre of the half-sphere.
- Apply the actuator load slowly combined with a sufficiently rapid data acquisition rate to have enough measurement points. Loading should be cyclical in steps. Pre-loading up to the maximum load is essential to eliminate connection clearance and determine its impact on the structure's geometry. If the difference in geometry between the prototype and the numerical model at the end of pre-loading is too significant, the numerical model must be adjusted.

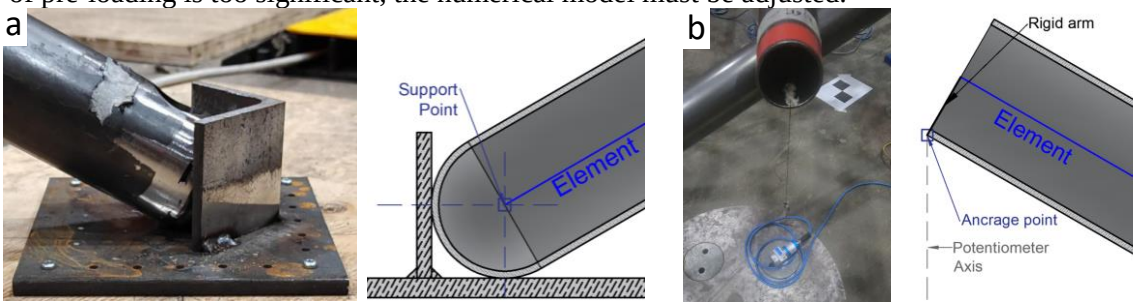

Figure 9: For 3D reciprocal structures, a proposition of (a) pinned support and (b) wire potentiometer sensor for displacement measurement is exposed. Each proposition is illustrated with (left) a picture in the laboratory and (right) a scheme specifying the numerical modelling.

Regarding instrumentation:

- Orient the sensors in the direction of the main component of displacement. For measuring displacements using LVDTs, ensure that the measured displacement component (e.g. vertical) is

significantly higher than the other components to limit interference. If this condition is not met, a solution, presented in Figure 9b, is to use a wire potentiometric sensor attached to the end of the tube. If the potentiometer is placed at a sufficient distance, its measurement will be minimally disturbed by other displacement components.

- Place the strain gauges along the same tube cross-section and determine the intensity and position of maximum stress in post-processing. This methodology allows comparison in terms of internal forces and stresses, improving the quality of result interpretation and helping the investigation of potential differences between experimental measurements and the numerical model. Indeed, for local stress computation, literature studies calculate von Mises stresses from point-wise measurements of rosette strain gauges placed on the tube. However, as reciprocity complexifies the structural behaviour, the position of maximum stress cannot always be estimated beforehand.

Acknowledgements

The authors thank Matthieu Tondeur and Justin Goosse for their assistance in the LEMSC testing laboratory (https://uclouvain.be/en/research-institutes/immc/lemsc).

References

[1] J. Geno, J. Goosse, S. Van Nimwegen, and P. Latteur, “Parametric design and robotic fabrication of whole timber reciprocal structures,” Autom. Constr., vol. 138, no. January, p. 104198, 2022, doi: 10.1016/j.autcon.2022.104198.

[2] D. Parigi and P. H. Kirkegaard, “The Reciprocalizer: An Agile Design Tool for Reciprocal Structures,” Nexus Netw. J., vol. 16, no. 1, pp. 61–68, 2014, doi: 10.1007/s00004-014-0176-x.

[3] Olga Popovic Larsen, RECIPROCAL FRAME ARCHITECTURE. Routledge, 2008.

[4] P. Latteur, J. Geno, and M. Vandamme, “Design rules for timber log reciprocal floors, based on mass optimization under stiffness constraint,” Int. J. Sp. Struct., vol. 36, no. 3, pp. 217–240, 2021, doi: 10.1177/09560599211041699.

[5] A. Pugnale and M. Sassone, “Structural Reciprocity: Critical Overview and Promising Research/Design Issues,” Nexus Netw. J., vol. 16, no. 1, pp. 9–35, 2014, doi: 10.1007/s00004-014-0174-z.

[6] Y. Anastas, L. Rhode-Barbarigos, and S. Adriaenssens, “Design-to-construction workflow for cell-based pattern reciprocal free-form structures,” J. Int. Assoc. Shell Spat. Struct., vol. 57, no. 2, pp. 159–176, 2016, doi: 10.20898/j.iass.2016.188.737.

[7] O. Baverel, “Nexorades: A family of interwoven space structures,” Univ. Surrey, no. December, pp. 1–323, 2000.

[8] P. Song, C. -Wing Fu, P. Goswami, J. Zheng, N. J. Mitra, and D. Cohen-Or, “Reciprocal frame structures made easy,” ACM Trans. Graph., vol. 32, no. 4, 2013, doi: 10.1145/2461912.2461915.

[9] E. Garavaglia, A. Pizzigoni, L. Sgambi, and N. Basso, “Collapse behaviour in reciprocal frame structures,” Struct. Eng. Mech., vol. 46, no. 4, pp. 533–547, 2013, doi: 10.12989/sem.2013.46.4.533.

[10] J. P. Rizzuto, “Experimental investigation of reciprocally supported element (RSE) lattice honeycomb domes structural behaviour,” Eng. Struct., vol. 166, no. February, pp. 496–510, 2018, doi: 10.1016/j.engstruct.2018.03.094.

[11] J. P. Rizzuto and R. Hulse, “Dodecahedric mutually supported element space structure: Experimental investigation,” Int. J. Sp. Struct., vol. 22, no. 2, pp. 107–121, 2007, doi: 10.1260/026635107781482640.

[12] J. P. Rizzuto, “Dodecahedric mutually supported element space structure: Numerical modelling,” J. Int. Assoc. Shell Spat. Struct., vol. 49, no. 157, pp. 3–18, 2008.

[13] J. P. Rizzuto, “Structural modelling investigation of reciprocally supported element lattice honeycomb domes,” Int. J. Comput. Methods Exp. Meas., vol. 5, no. 4, pp. 432–441, 2017, doi: 10.2495/CMEM-V5-N4-432-441.

[14] X. Iriarte, J. Aginaga, G. Gainza, J. Ros, and J. Bacaicoa, “Optimal strain-gauge placement for mechanical load estimation in circular cross-section shafts,” Meas. J. Int. Meas. Confed., vol. 174, no. April 2020, p. 108938, 2021, doi: 10.1016/j.measurement.2020.108938.